

Designer Topological Insulator with Enhanced Gap and Suppressed Bulk Conduction in Bi₂Se₃/Sb₂Te₃ Ultrashort-Period Superlattices

Ido Levy, Cody Youmans, Thor Axtmann Garcia, Haiming Deng, Steven Alsheimer, Christophe Testelin, Lia Krusin-Elbaum, Pouyan Ghaemi, and Maria C. Tamargo*

Cite This: Nano Lett. 2020, 20, 3420–3426

Read Online



ACCESS



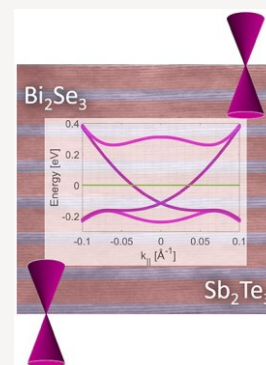
Metrics & More



Article Recommendations

* Supporting Information

ABSTRACT: A novel approach to suppress bulk conductance in three-dimensional (3D) topological insulators (TIs) using short-period superlattices (SLs) of two TIs is presented. Evidence for superlattice gap enhancement (SGE) was obtained from the reduction of bulk background doping from $1.2 \times 10^{20} \text{ cm}^{-3}$ to $8.5 \times 10^{18} \text{ cm}^{-3}$ as the period of Bi₂Se₃/Sb₂Te₃ SLs is decreased from 12 nm to 5 nm. Tight binding calculations show that, in the ultrashort-period regime, a significant SGE can be achieved for the resulting SL. Ultrathin short-period SLs behave as new designer TIs with bulk bandgaps up to 60% larger than the bandgap of the constituent layer of largest bandgap, while retaining topological surface features. Evidence for gap formation was obtained from ellipsometric measurements. Analysis of the weak antilocalization cusp in low-temperature magneto-conductance confirms that the top and bottom surfaces of the SL structure behave as Dirac surfaces. This approach represents a promising platform for building truly insulating TIs.



KEYWORDS: topological insulator, molecular beam epitaxy, superlattice, gap enhancement, Bi₂Se₃, Sb₂Te₃

There is currently much excitement around the novel devices^{17,18} for decades. In the field of topological materials, physics and potential device applications of three- attempts to combine TI layers with trivial semiconductors or dimensional (3D) topological insulators (TIs).^{1–3} A bandgap combining two topologically trivial materials to get 3D TIs has in the bulk, which renders them bulk insulators, along with been explored. Recently, SLs of Bi₂Se₃/In₂Se₃^{19–21} have shown metallic helical surface states are the principal properties that that the bandgap and the Dirac cone of the Bi₂Se₃ could be garner interest in their research. The TI surface provides a modified by the SL structure. Another system, ZnCdSe/Bi₂Se₃ novel electronic state that would harvest exotic quasi-particles, SLs, showed multiple topological surface channels that scale such as Majorana Fermions, and other phenomena.^{4–6} with the number of SL periods.²² A few examples of the growth Groundbreaking potential applications such as quantum and properties of heterojunctions and SLs comprised of two TI computing are envisioned.⁷ The most widely studied of these materials, such as Bi₂Te₃/Sb₂Te₃, have also been previously materials is Bi₂Se₃, because of its relatively large bandgap and reported;^{23–26} however, the effect of short-period TI/TI SLs single surface Dirac cone, but other group V-chalcogenides on the band structure and carrier density of the resulting

such as Bi_2Te_3 and Sb_2Te_3 are also of great interest.⁸

Despite their attractive properties, the relatively small bandgap of these materials of a few hundred millielectron volts, and the ease of formation of electrically active defects⁹ result in high bulk conductivities, masking the features of their exotic surface states. In particular, when grown by molecular beam epitaxy (MBE), bulk Bi_2Se_3 is n-type¹⁰ and Sb_2Te_3 is p-type.¹¹ Many attempts to reduce the bulk carrier density in TIs have been reported, including modification of the growth conditions and the substrates used,^{11,12} impurity compensation

13–15

16

doping, and the growth of mixed alloys. Despite observed reduction of bulk conductivity through these methods, it is evident that significant improvement toward truly insulating bulk TIs requires the invention of fundamentally new protocols.

Band structure engineering by superlattice (SL) formation

has been widely applied to semiconductor physics and

materials, or on their topological surface states, has not been appreciably addressed.

In this work, we report the growth of short-period SLs of alternating Bi_2Se_3 and Sb_2Te_3 , (TI/TI SLs) which have a type III or “broken gap” band alignment. In type III band alignment, both the valence and the conduction band extrema of one of the constituent materials lie above or below those of the other one, and the bandgaps of the two materials do not overlap.²⁷ The TI SL structures show a reduction of the bulk



© 2020 American Chemical Society

3420

<https://dx.doi.org/10.1021/acs.nanolett.0c00338>

Nano Lett. 2020, 20, 3420–3426

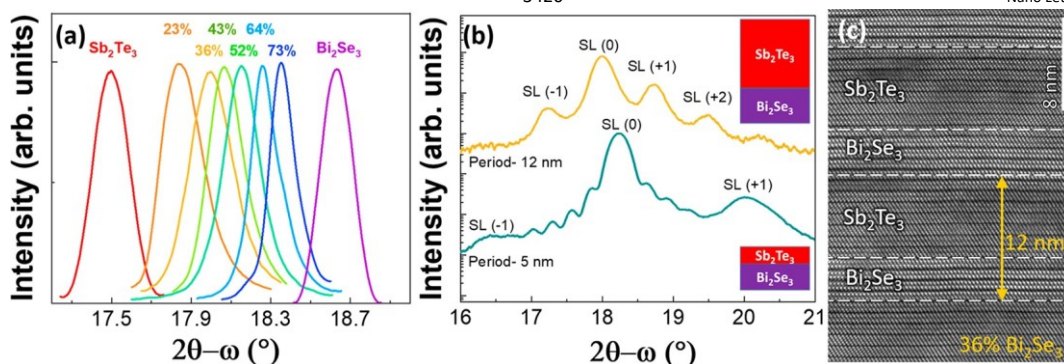


Figure 1. (a) XRD measurements of the (006) zero-order SL peaks of several of the SL samples studied and of pure Bi_2Se_3 and Sb_2Te_3 . The peak position varied between that of the two pure materials, providing a measure of the average composition of the SL. The colors of the spectra, transitioning from purple to red, illustrate the gradual change in effective composition from pure Bi_2Se_3 to pure Sb_2Te_3 . (b) Full HRXRD scans of the (006) plane of the sample with 36% Bi_2Se_3 effective composition (top) and 52% effective composition (bottom). From the position of the SL satellite peaks [SL(+1) SL(-1) SL(+2)] the period of the SL could be calculated. Insets show the period thicknesses with proportional layer thicknesses calculated from XRD. (c) HRTEM cross-section image of the sample with 36% Bi_2Se_3 effective composition showing the alternating materials.

carrier density and an increase of the bulk resistivity as a function of the SL period thickness, while still retaining the topological surface states. We interpret this as evidence of new bulk bandgap formation in the SL material that increases with reduced period thickness. Tight binding calculations confirm that, for certain materials parameters and TI/TI SL periods, new “designer” 3D TI phases can be achieved with bulk bandgaps significantly larger than the bandgaps of either of the constituent layers. This novel approach to materials design and band structure engineering offers much promise for the realization of new TI materials with wider bandgaps than those available in bulk TIs and represents a promising and novel platform for building truly insulating bulk topological materials.

A series of SL samples consisting of alternating thin layers of Bi_2Se_3 and Sb_2Te_3 were grown by MBE and their structural properties were investigated using high-resolution X-ray diffraction (HRXRD) and transmission electron microscopy (TEM). The SL structures were grown on a

Bi_2Se_3 buffer layer on (0001) c-plane sapphire substrates with a 0.2° off-cut. A Riber 2300P MBE system was used with background pressures of $3\text{--}5 \times 10^{-10}$ Torr during growth. Samples with different SL period thicknesses, as well as different ratios of individual Bi_2Se_3 to Sb_2Te_3 layer thickness, were grown. All samples consist of seven periods of the two alternating materials. The samples were grown using our previously reported MBE growth procedure that ensures very smooth and almost twin free single-layer crystals.²⁸ Details of the growth are presented in the Supporting Information.

Scans of the HRXRD (006) reflection of the zero-order SL peak, SL(0), (Figure 1a), and the superlattice satellite peaks (Figure 1b) allowed us to calculate the effective composition of each sample, the thickness of the SL period,²⁹ and the individual thicknesses of the Bi_2Se_3 and Sb_2Te_3 layers. The HRXRD measurements were performed using a Bruker D8 Discover diffractometer with a da Vinci configuration and a $\text{Cu K}\alpha_1(1.5418 \text{ \AA})$ source to establish their crystal quality.

The good structural quality was also confirmed by the high-resolution transmission electron microscopy (HRTEM) image of the sample with 36% Bi_2Se_3 effective composition, which consisted of 4 nm Bi_2Se_3 and 8 nm Sb_2Te_3 , as deduced from the HRXRD data. TEM measurements were performed (EAG Laboratories) using a Hitachi HD-2700 Spherical AberrationCorrected Scanning-TEM system coupled with energydispersive X-ray spectroscopy (EDS). The TEM image (Figure 1c) shows alternating layers with different contrast indicating the two different materials: the lighter contrast corresponding to the Bi_2Se_3 layer and the darker one corresponding to the Sb_2Te_3 layer. The calculated TEM thickness values agree well with the layer thicknesses extracted from the HRXRD measurements. In addition, the HRTEM image clearly displays the quintuple layer (QL) structure of the individual layers, as well as the high crystallinity of the structure. Although atomically well-ordered, the interfaces show some interface steps, or interface roughness, which appears more pronounced on the surfaces of the Sb_2Te_3 layers, consistent with observations that MBE grown Sb_2Te_3 has a higher degree of roughness than Bi_2Se_3 .^{11,30}

Transport of all the samples was investigated by Hall effect measurements, at 10K, using the van der Pauw³¹ (vdP) configuration with indium contacts on a Lakeshore 7600 electromagnet system. The plot of the Hall resistance (R_{xy}), as a function of magnetic field (B), was used to learn the sample conductivity type (n- or p-type). All the samples were measured. Several representative plots are shown in Figure 2a. The corresponding effective composition for each sample is given in the figure. The sign of the slope dictates the conductivity type. We observed a transition of the SL conductivity from n-type to p-type at an effective Bi_2Se_3 composition of ~42%.

Carrier density for all of the samples was also obtained from the Hall measurements at 10 K. The bulk carrier density (carriers per cm^3) is plotted to correct for variations in total SL thickness among the samples. The data is plotted as a function of the % Bi_2Se_3 effective composition in Figure 2b. In this analysis, it was anticipated that the carrier density would reach a minimum at the transition region between n-type to p-type behavior, as charge neutrality was achieved. This transition region is indicated in the figure by the bright vertical region in the background separating the p-type samples from the n-type samples. However, no reduction in the carrier density near the transition region was evident in the data, suggesting that other factors are affecting the variations in conductivity of the samples. In fact, no correlation of carrier density with % Bi_2Se_3

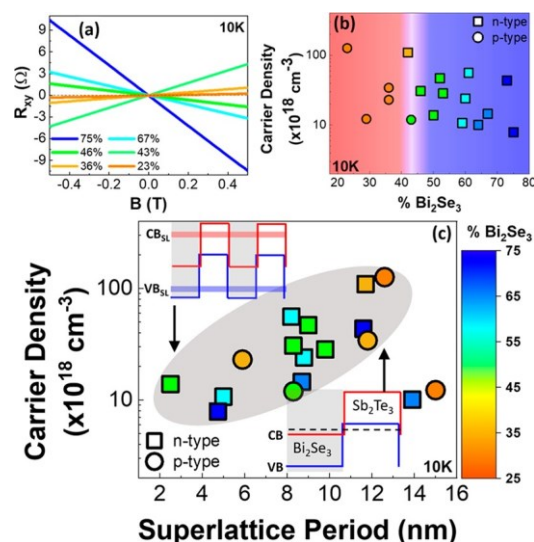


Figure 2. (a) Hall resistance plots of the SL samples. The effective composition is listed in the legend and illustrated by the color of the lines, as assigned in Figure 1a. (b) Carrier concentration of the samples as a function of the % Bi_2Se_3 effective composition. The bright vertical region indicates the composition at which the SL behavior changes from p-type (red background) to n-type (blue background). (c) Carrier concentration of the samples, as a function of the SL period thickness (shaded region is drawn to aid the eye). The color of the symbols in panels (b) and (c) corresponds to the effective compositions, as indicated in the bar of panel (c). Insets illustrate the type III band alignment between Bi_2Se_3 and Sb_2Te_3 and band diagram of the SL. The small-period SL results in the formation of a SL gap, which can be tuned by the period and layer thicknesses.

effective composition was evident in either the n-type samples (squares in Figure 2) or the p-type samples (circles in Figure 2).

By contrast, a strong correlation is noted in Figure 2c, where the carrier density is plotted as a function of the SL period. Although most of the samples studied are n-type (only five ptype samples were grown), both carrier types display a similar relationship. A reduced carrier density for the samples with smaller SL periods is clearly observed. More than an order of magnitude reduction in carrier density was obtained between the samples with larger periods (~12 nm) and those with smaller periods (~3 nm). The two data points for samples with a period above 14 nm do not follow this trend, and have been excluded from our discussion since, at sufficiently large layer thickness, a superlattice behavior may no longer apply. The low carrier densities of our smaller-period TI/TI SLs are comparable to the best values reported for the constituent TI materials grown by MBE directly on sapphire substrates.^{11,12,32,33} We believe that these values can be significantly improved, as these results were achieved only by our first efforts. We propose that mastering the properties of TI/TI SLs provides

a promising and yet-to-be-explored platform for building truly insulating topological materials.

These observations can be understood based on simple band structure considerations. The heterostructure band alignments between Bi_2Se_3 and Sb_2Te_3 are illustrated in the insets of Figure 2c. As previously noted, these two materials have a type III, or “broken gap” band alignment,^{34,35} and the MBE-grown Sb_2Te_3 is p-type, while the Bi_2Se_3 is n-type.⁹ As portrayed in the insets, the generation of a SL with small enough periodicity modifies the band structure and produces new gaps that can be tuned by changing the SL period and thickness.³⁶

A better understanding of the properties of these short period TI/TI SLs, and the possibilities of band structure engineering in these novel materials can be obtained from tight binding calculations. Since the alternating layers consist of only a few single layers of each material, we are effectively developing a new type of material and tight binding is the appropriate method to derive the band structure of our new compound.

The low-energy properties of both Bi_2Se_3 and Sb_2Te_3 are well-described by the effective k·p Hamiltonian introduced by Zhang et al.³⁷ Using the parameters from ref 38, we built a tight-binding model Hamiltonian. Figure 3a shows the resulting highest valence and lowest conduction bands for a SL with $n(\text{Bi}_2\text{Se}_3) = 1$ QL and $n(\text{Sb}_2\text{Te}_3) = 1$ QL, compared with those of pure Bi_2Se_3 and Sb_2Te_3 . The figure highlights an instance of the large superlattice gap enhancement (SGE) expected from the experiments detailed above. A bulk SL bandgap as high as ~160% of the constituent material with the largest bandgap is predicted in Figure 3b, supporting the proposal of significantly increased bandgaps with decreasing period thickness. It is important to note that the material described by the calculation, consisting of a few QL of Sb_2Te_3 and a few QLs of Bi_2Se_3 can no longer be considered as alternating layers of the two bulk materials, as our simple diagrams of Figure 2c suggest (as k·p calculations would do), but rather as a new “designer” 3D material. Figure 3c demonstrates the preserved topological nature of the composite material by displaying the edge bands at a particular termination of the SL (Bi_2Se_3 in our case), within the corresponding bulk band gap. Furthermore, in contrast with the two constituent materials, the Fermi level in the resulting SL sample lies midgap and near the Dirac point, as desired for achieving truly insulating TIs. Thus, the new designer material formed by alternating thin layers of two constituent TIs is itself a new 3D TI with preserved topological surface states at the top and bottom surfaces of the SL, whose bulk bandgap increases as the period of the superlattice layers decreases. Details of the tight binding methodology are given in the Supporting Information.

To confirm the formation of a new bulk bandgap and subsequent gap enhancement, we have performed ellipsometric measurements on different SLs and on a reference Sb_2Te_3 layer, which is an approach that was recently used to study Bi_2Se_3 gap energy^{39,40} (the experimental procedure is described in the Supporting

Information). Figure 3d shows the imaginary component of the dielectric function (related to absorption) versus photon energy, measured for a 5-QL-period SL (2 Sb_2Te_3 QL – 3 Bi_2Se_3 QL). This curve is very similar to what was measured on $\text{Bi}_2\text{Se}_{3-x}\text{Te}_x$ epitaxial layers.³⁹ An onset, well determined by plotting the second derivative, $\frac{d^2\epsilon_2}{dE^2}$, is

observed at an energy $E_{\text{opt}} = 403 \pm 10$ meV. From this optical transition and the SL n-doping, it is possible to estimate the SL gap (E_{gap}) in the range of 236 ± 36 meV. This gap energy can be compared with that of Sb_2Te_3 (232 meV), also measured by ellipsometry, leading to a SGE value of $102\% \pm 16\%$, which is very close to the predicted value of 105% (see Figure 3b). By contrast, similar measurements on a sample with a period of 8 QL showed no evidence of a transition within the explored energy range, consistent with a gap of ~70 meV or less, also

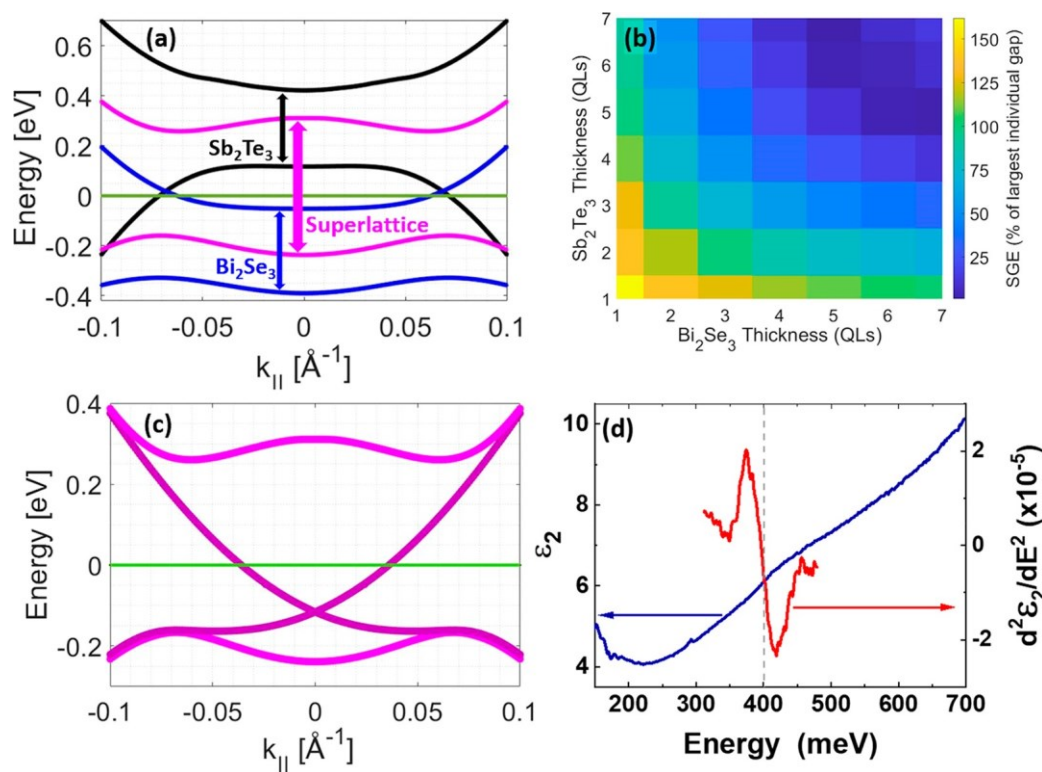


Figure 3. (a) Bulk band gaps of Bi_2Se_3 (blue), Sb_2Te_3 (black), and an ultrathin binary SL (magenta) of Bi_2Se_3 and Sb_2Te_3 with respective layer thicknesses $n(\text{Bi}_2\text{Se}_3) = 1$ QL and $n(\text{Sb}_2\text{Te}_3) = 1$ QL. (b) SGE dependence on short-period SL layer thicknesses. (c) Bulk gap and subgap edge bands of the SL considered in panel (a). (d) Imaginary component of the dielectric constant ϵ_2 and its second derivative $d^2\epsilon_2/dE^2$, at room temperature, dE for a SL with a period of 5 QL. A dashed line indicates the optical onset (E_{opt}), clearly identified by the inflection point of the second derivative curve.

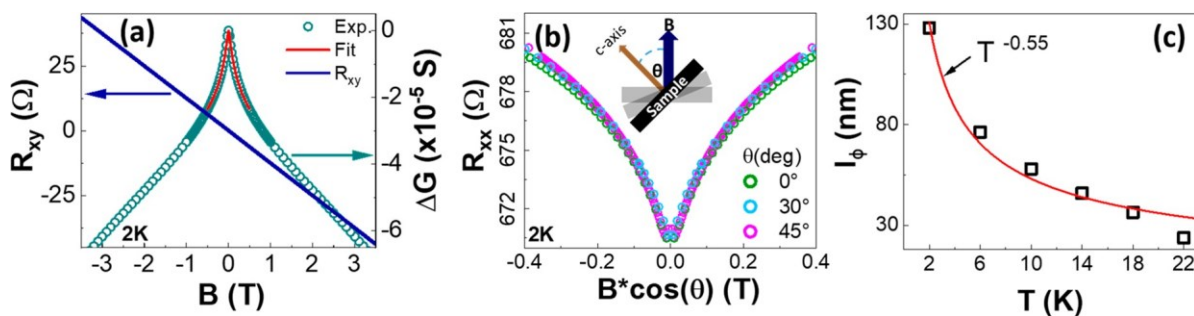


Figure 4. (a) Magneto-conductance of the sample with a 5 nm SL period thickness, showing a weak antilocalization (WAL) cusp. A fit to the HLN theory, shown in red, gives a value of $\alpha = 1$. Hall resistance for the sample is also shown as a function of the magnetic field (B). (b) Angledependent magnetoresistance of the 5-nm-period SL, as a function of the transverse component of magnetic field, $B_\perp = B \cdot \cos(\theta)$. (c) Temperature dependence of dephasing length l_ϕ for the same sample as in panels (a) and (b).

predicted by the model. (See Figure S3 in the Supporting Information.)

In order to investigate experimentally the presence of the topologically nontrivial surface states in these new “designer” TI/TI SLs, as predicted by the tight binding calculations, magneto-conductance (M-C) measurements were performed at 2 K on the sample with a period of 5 nm. The M-C measurements were performed in a 14 T Quantum Design physical property measurement system (PPMS) in 1 mTorr (at low temperature) of He gas. Electrical contacts in the vdP configuration were made with indium bonded on the

edge of the thin film. The M-C measurements, shown in Figure 4a, exhibit a weak antilocalization (WAL) cusp, which is the trademark of 2D transport channels.^{41,42} The plot of the Hall resistance for the same sample is also shown displaying a highly linear behavior consistent with single carrier behavior.⁴³ Additional details can be found in the Supporting Information.

Further analysis of the data was performed by fitting to the Hikami–Larkin–Nagaoka (HLN) two-dimensional (2D) localization theory.⁴⁴ From this fit, we extracted a value to the fitting parameter α of 1.0 for the small-period (5 nm)

sample. It has been shown that the parameter α is proportional to the number of 2D channels in the layer, where $\alpha = 0.5$ represents one channel. Our results suggest that the SL sample behaves like a new 3D TI material with only the top and bottom surfaces of the structure hosting topological surface states.

Angle-dependent magneto-resistance for the same sample are presented in Figure 4b, where the magneto-resistance, measured with the magnetic field at different angles (θ) normal to the sample surface, is plotted as a function of the transverse component of the magnetic field. All of the plots collapse to one curve, suggesting that the 2D conductance channels resulted from the surface electrons. Finally, the M-C as a function of temperature was also measured. The dephasing length (l_ϕ), plotted as a function of temperature, is shown in Figure 4c. The data well-fit a temperature dependence of $T^{-0.55}$, very close to the ideal $T^{-0.5}$ dependence predicted by HLN theory for 2D conduction channels.⁴⁵ This reinforces our conclusion that the SL sample behaves as a new “designer” 3D TI phase with a bandgap in the bulk and topological surface states at the top and bottom surfaces of the sample. Furthermore, the residual bulk conductivity of the new “designer” TI material can be adjusted by the appropriate choice of SL parameters, because of a large SGE possible for ultrathin period SLs.

This work presents a novel approach to band structure engineering and reduced background doping of topological insulators by the use of ultrathin period TI/TI SLs. An observed reduction of bulk background doping by more than one order of magnitude, as the period of the SLs decreases from 12 nm to less than 5 nm, can be understood on the basis of a SGE possible in type III “broken gap” heterostructures. This interpretation is supported by tight binding calculations, and experimentally confirmed by optical ellipsometry. We show, from M-C measurements, that the topological surface states of the grown TI/TI SL with the 5-QL period are, in fact, preserved. Thus, a new “designer” 3D topological insulator material with enhanced bulk bandgap and preserved helical surface states is produced. This approach represents a promising and yet-to-be-explored novel platform for building truly insulating bulk topological materials.

ASSOCIATED CONTENT

* Supporting Information

The Supporting Information is available free of charge at <https://pubs.acs.org/doi/10.1021/acs.nanolett.0c00338>.

Additional information and figures related to the growth and structural characterization, transport measurements, optical measurements, and theoretical modeling (PDF)

AUTHOR INFORMATION

Corresponding Author

Maria C. Tamargo – Department of Chemistry, The City College of New York, New York, New York 10031, United States; Chemistry Program and Physics Program, Graduate Center of CUNY, New York, New York 10021, United States; orcid.org/0000-0002-2991-2674; Email: mtamargo@ccny.cuny.edu

Authors

Ido Levy – Department of Chemistry, The City College of New York, New York, New York 10031, United States; Chemistry Program, Graduate Center of CUNY, New York, New York 10021, United States; orcid.org/0000-0002-3962-4393

Cody Youmans – Department of Physics, The City College of New York, New York, New York 10031, United States; Physics Program, Graduate Center of CUNY, New York, New York 10021, United States

Thor Axtmann Garcia – Department of Chemistry, The City College of New York, New York, New York 10031, United States; Chemistry Program, Graduate Center of CUNY, New York, New York 10021, United States

Haiming Deng – Department of Physics, The City College of New York, New York, New York 10031, United States; Physics Program, Graduate Center of CUNY, New York, New York 10021, United States

Steven Alsheimer – Department of Physics, The City College of New York, New York, New York 10031, United States

Christophe Testelin – Sorbonne Universite, CNRS, Institut des NanoSciences de Paris, F-75005 Paris, France

Lia Krusin-Elbaum – Department of Physics, The City College of New York, New York, New York 10031, United States; Physics Program, Graduate Center of CUNY, New York, New York 10021, United States

Pouyan Ghaemi – Department of Physics, The City College of New York, New York, New York 10031, United States; Physics Program, Graduate Center of CUNY, New York, New York 10021, United States

Complete contact information is available at: <https://pubs.acs.org/10.1021/acs.nanolett.0c00338>

Author Contributions

I.L., T.A.G., and M.C.T. conceived the experiment and executed the crystal growth. I.L. performed HRXRD and XRR measurements. S.A. and I.L. performed and analyzed the 10 K Hall effect measurements. H.D. and L.K.-E. performed the 2 K magneto conductance measurements. C.Y. and P.G. conducted the analytical theoretical modeling. C.T. and I.L. performed and analyzed the optical measurements. I.L., C.Y., P.G., C.T., and M.C.T. wrote and reviewed the manuscript. All authors contributed to interpretation of the data and discussions.

Notes

The authors declare no competing financial interest.

ACKNOWLEDGMENTS

This work was supported by NSF (Grant Nos. DMR-1420634 (MRSEC PAS³), HRD-1547830 (IDEALS CREST), and DMR-1824265). We gratefully acknowledge valuable discussions and input from A. N. Pasupathy and C. Rubio Verdú.

REFERENCES

- (1) Qi, X. L.; Zhang, S. C. The quantum spin Hall effect and topological insulators. *Phys. Today* 2010, 63, 33–38.
- (2) Hasan, M. Z.; Kane, C. L. Colloquium: Topological insulators. *Rev. Mod. Phys.* 2010, 82, 3045–3067.
- (3) Qi, X. L.; Zhang, S. C. Topological insulators and superconductors. *Rev. Mod. Phys.* 2011, 83, 1057–1110.
- (4) Fu, L.; Kane, C. L. Superconducting proximity effect and Majorana fermions at the surface of a topological insulator. *Phys. Rev. Lett.* 2008, 100, 096407.
- (5) Stanescu, T. D.; Sau, J. D.; Lutchyn, R. M.; Das Sarma, S. Proximity effect at the superconductor-topological insulator interface. *Phys. Rev. B: Condens. Matter Mater. Phys.* 2010, 81, 241310.
- (6) Read, N. Topological phases and quasiparticle braiding. *Phys. Today* 2012, 65, 38–43.
- (7) Moore, J. E. The birth of topological insulators. *Nature* 2010, 464, 194–198.
- (8) Zhang, H.; Liu, C. X.; Qi, X. L.; Dai, X.; Fang, Z.; Zhang, S. C. Topological insulators in Bi₂Se₃, Bi₂Te₃ and Sb₂Te₃ with a single Dirac cone on the surface. *Nat. Phys.* 2009, 5, 438–442.
- (9) West, D.; Sun, Y. Y.; Wang, H.; Bang, J.; Zhang, S. B. Native defects in second-generation topological insulators: Effect of spinorbit interaction on Bi₂Se₃. *Phys. Rev. B: Condens. Matter Mater. Phys.* 2012, 86, 121201.
- (10) He, L.; Xiu, F.; Wang, Y.; Fedorov, A. V.; Huang, G.; Kou, X.; Lang, M.; Beyermann, W. P.; Zou, J.; Wang, K. L. Epitaxial growth of Bi₂Se₃ topological insulator thin films on Si (111). *J. Appl. Phys.* 2011, 109, 103702.
- (11) Thiet, D. V.; Quang, V. N.; Hai, N. T. M.; Huong, N. T.; Cho, S.; Tuan, D. A.; Dung, D. D.; Tam, T. V. Optimizing the carrier density and thermoelectric properties of Sb₂Te₃ films by using the growth temperature. *J. Korean Phys. Soc.* 2018, 72, 915–919.
- (12) Koirala, N.; Brahlek, M.; Salehi, M.; Wu, L.; Dai, J.; Waugh, J.; Nummy, T.; Han, M. G.; Moon, J.; Zhu, Y.; Dessau, D.; Wu, W.; Armitage, N. P.; Oh, S. Record surface state mobility and quantum Hall effect in topological insulator thin films via interface engineering. *Nano Lett.* 2015, 15, 8245–8249.
- (13) Hong, S. S.; Cha, J. J.; Kong, D.; Cui, Y. Ultra-low carrier concentration and surface-dominant transport in antimony-doped Bi₂Se₃ topological insulator nanoribbons. *Nat. Commun.* 2012, 3, 757.
- (14) Chen, Y. L.; Analytis, J. G.; Chu, J.-H.; Liu, Z. K.; Mo, S. K.; Qi, X. L.; Zhang, H. J.; Lu, D. H.; Dai, X.; Fang, Z.; Zhang, S. C.; Fisher, I. R.; Hussain, Z.; Shen, Z.-X. Experimental realization of a three-dimensional topological insulator, Bi₃Te₂. *Science* 2009, 325, 178–181.
- (15) Ginley, T. P.; Wang, Y.; Law, S. Topological insulator film growth by molecular beam epitaxy: A review. *Crystals* 2016, 6, 154.
- (16) Bao, L.; He, L.; Meyer, N.; Kou, X.; Zhang, P.; Chen, Z. G.; Fedorov, A. V.; Zou, J.; Riedemann, T. M.; Lograsso, T. A.; Wang, K. L.; Tuttle, G.; Xiu, F. Weak antilocalization and quantum oscillations of surface states in topological insulator Bi₂Se₂Te. *Sci. Rep.* 2012, 2, 726.
- (17) Esaki, L.; Chang, L. L. New transport phenomenon in a semiconductor “superlattice”. *Phys. Rev. Lett.* 1974, 33, 495–498.
- (18) Fox, M.; Ispasoiu, R. Quantum wells, superlattices, and bandgap engineering. In *Springer Handbook of Electronic and Photonic Materials*; Kasap, S., Capper, P., Eds.; Springer: Cham, Switzerland, 2017.
- (19) Belopolski, I.; Xu, S. Y.; Koirala, N.; Liu, C.; Bian, G.; Strocov, V. N.; Chang, G.; Neupane, M.; Alidoust, N.; Sanchez, D.; Zheng, H.; Brahlek, M.; Rogalev, V.; Kim, T.; Plumb, N. C.; Chen, C.; Bertran, F.; Le Fevre, P.; Taleb-Ibrahimi, A.; Asensio, M. C.; Shi, M.; Lin, H.; Hoesch, M.; Oh, S.; Hasan, M. Z. A novel artificial condensed matter lattice and a new platform for one-dimensional topological phases. *Sci. Adv.* 2017, 3, No. e1501692.
- (20) Wang, Z. Y.; Guo, X.; Li, H. D.; Wong, T. L.; Wang, N.; Xie, M. H. Superlattices of Bi₂Se₃/In₂Se₃: Growth characteristics and structural properties. *Appl. Phys. Lett.* 2011, 99, 023112.
- (21) Zhao, Y.; Liu, H.; Guo, X.; Jiang, Y.; Sun, Y.; Wang, H.; Wang,

- Y.; Li, H. D.; Xie, M. H.; Xie, X. C.; Wang, J. Crossover from 3D to 2D quantum transport in $\text{Bi}_2\text{Se}_3/\text{In}_2\text{Se}_3$ superlattices. *Nano Lett.* 2014, 14, 5244–5249.
- (22) Chen, Z.; Zhao, L.; Park, K.; Garcia, T. A.; Tamargo, M. C.; Krusin-Elbaum, L. Robust topological interfaces and charge transfer in epitaxial $\text{Bi}_2\text{Se}_3/\text{II-VI}$ semiconductor superlattices. *Nano Lett.* 2015, 15, 6365–6370.
- (23) Narendra, N.; Kim, K. W. Toward enhanced thermoelectric effects in $\text{Bi}_2\text{Te}_3/\text{Sb}_2\text{Te}_3$ heterostructures. *Semicond. Sci. Technol.* 2017, 32, 035005.
- (24) Touzelbaev, M. N.; Zhou, P.; Venkatasubramanian, R.; Goodson, K. E. Thermal characterization of $\text{Bi}_2\text{Te}_3/\text{Sb}_2\text{Te}_3$ superlattices. *J. Appl. Phys.* 2001, 90, 763–767.
- (25) Hinsche, N. F.; Yavorsky, B. Y.; Gradhand, M.; Czerner, M.; Winkler, M.; Konig, J.; Bottner, H.; Mertig, I.; Zahn, P. Thermoelectric transport in $\text{Bi}_2\text{Te}_3/\text{Sb}_2\text{Te}_3$ superlattices. *Phys. Rev. B: Condens. Matter Mater. Phys.* 2012, 86, 085323.
- (26) Lanius, M.; Kampmeier, J.; Weyrich, C.; Kölling, S.; Schall, M.; Schüffelgen, P.; Neumann, E.; Luysberg, M.; Mussler, G.; Koenraad, P. M.; SchaPers, T.; Grützmacher, D. P–N junctions in ultrathin topological insulator $\text{Sb}_2\text{Te}_3/\text{Bi}_2\text{Te}_3$ heterostructures grown by molecular beam epitaxy. *Cryst. Growth Des.* 2016, 16, 2057–2061.
- (27) Plis, E. InAs/GaSb type-II superlattice detectors. *Adv. Electron.* 2014, 2014, 246769.
- (28) Levy, I.; Garcia, T. A.; Shafique, S.; Tamargo, M. C. Reduced twinning and surface roughness of Bi_2Se_3 and Bi_2Te_3 layers grown by molecular beam epitaxy on sapphire substrates. *J. Vac. Sci. Technol., B: Nanotechnol. Microelectron.: Mater., Process., Meas., Phenom.* 2018, 36, 02D107.
- (29) Vandenberg, J. M.; Hamm, R. A.; Macrander, A. T.; Panish, M. B.; Temkin, H. Structural characterization of GaInAs(P)/InP quantum well structures grown by gas source molecular beam epitaxy. *Appl. Phys. Lett.* 1986, 48, 1153–1155.
- (30) Richardella, A.; Zhang, D. M.; Lee, J. S.; Koser, A.; Rench, D. W.; Yeats, A. L.; Buckley, B. B.; Awschalom, D. D.; Samarth, N. Coherent heteroepitaxy of Bi_2Se_3 on GaAs (111)B. *Appl. Phys. Lett.* 2010, 97, 262104.
- (31) van der Pauw, L. J. A method for measuring the resistivity and Hall coefficient on lamellae of arbitrary shape. *Philips Technol. Rev.* 1958, 20, 220–224.
- (32) Satake, Y.; Shiogai, J.; Takane, D.; Yamada, K.; Fujiwara, K.; Souma, S.; Sato, T.; Takahashi, T.; Tsukazaki, A. Fermi-level tuning of the Dirac surface state in $(\text{Bi}_{1-x}\text{Sb}_x)_2\text{Se}_3$ thin films. *J. Phys.: Condens. Matter* 2018, 30, 085501.
- (33) Tabor, P.; Keenan, C.; Urazhdin, S.; Lederman, D. Molecular beam epitaxy and characterization of thin Bi_2Se_3 films on Al_2O_3 (110). *Appl. Phys. Lett.* 2011, 99, 013111.
- (34) Takane, D.; Souma, S.; Sato, T.; Takahashi, T.; Segawa, K.; Ando, Y. Work function of bulk-insulating topological insulator $\text{Bi}_{2-x}\text{Sb}_x\text{Te}_{3-y}\text{Se}_y$. *Appl. Phys. Lett.* 2016, 109, 091601.
- (35) Menshchikova, T. V.; Otrokov, M. M.; Tsirkin, S. S.; Samorokov, D. A.; Bebneva, V. V.; Ernst, A.; Kuznetsov, V. M.; Chulkov, E. V. Band structure engineering in topological insulator based heterostructures. *Nano Lett.* 2013, 13, 6064–6069.
- (36) Zakharova, A.; Yen, S. T.; Chao, K. A. Strain-induced semimetal-semiconductor transition in InAs/GaSb broken-gap quantum wells. *Phys. Rev. B: Condens. Matter Mater. Phys.* 2002, 66, 085312.
- (37) Liu, C. X.; Qi, X. L.; Zhang, H.; Dai, X.; Fang, Z.; Zhang, S. C. Model Hamiltonian for topological insulators. *Phys. Rev. B: Condens. Matter Mater. Phys.* 2010, 82, 045122.
- (38) Nechaev, I. A.; Krasovskii, E. E. Relativistic $\mathbf{k} \cdot \mathbf{p}$ Hamiltonians for centrosymmetric topological insulators from ab initio wave functions. *Phys. Rev. B: Condens. Matter Mater. Phys.* 2016, 94, No. 201410(R).
- (39) Dubroka, A.; Caha, O.; Hroncek, M.; Fris, P.; Orlita, M.; Holy, V.; Steiner, H.; Bauer, G.; Springholz, G.; Humlicek, J. Interband absorption edge in the topological insulators $\text{Bi}_2(\text{Te}_{1-x}\text{Se}_x)_3$. *Phys. Rev. B: Condens. Matter Mater. Phys.* 2017, 96, 235202.
- (40) Post, K. W.; Chapler, B. C.; He, L.; Kou, X.; Wang, K. L.; Basov, D. N. Thickness-dependent bulk electronic properties in Bi_2Se_3 thin films revealed by infrared spectroscopy. *Phys. Rev. B: Condens. Matter Mater. Phys.* 2013, 88, 075121.
- (41) Steinberg, H.; Laloe, J. B.; Fatemi, V.; Moodera, J. S.; JarilloHerrero, P. Electrically tunable surface-to-bulk coherent coupling in topological insulator thin films. *Phys. Rev. B: Condens. Matter Mater. Phys.* 2011, 84, 233101.
- (42) Chen, J.; He, X. Y.; Wu, K. H.; Ji, Z. Q.; Lu, L.; Shi, J. R.; Smet, J. H.; Li, Y. Q. Tunable surface conductivity in Bi_2Se_3 revealed in diffusive electron transport. *Phys. Rev. B: Condens. Matter Mater. Phys.* 2011, 83, No. 241304(R).
- (43) Eschbach, M.; Mlynczak, E.; Kellner, J.; Kampmeier, J.; Lanius, M.; Neumann, E.; Weyrich, C.; Gehlmann, M.; Gospodaric, P.; Doring, S.; et al. Realization of a vertical topological p–n junction in epitaxial $\text{Sb}_2\text{Te}_3/\text{Bi}_2\text{Te}_3$ heterostructure. *Nat. Commun.* 2015, 6, 8816. (44) Hikami, S.; Larkin, A. I.; Nagaoka, Y. Spin-orbit interaction and magnetoresistance in the two dimensional random system. *Prog. Theor. Phys.* 1980, 63, 707–710.
- (45) Altshuler, B. L.; Aronov, A. G.; Khmel'nitsky, D. E. Effects of electron-electron collisions with small energy transfers on quantum localisation. *J. Phys. C: Solid State Phys.* 1982, 15, 7367–7386.